

# Enhanced spatially-resolved trace analysis using combined SIMS–single-stage AMS



K.S. Grabowski<sup>a,\*</sup>, E.E. Groopman<sup>b</sup>, A.J. Fahey<sup>c</sup>

<sup>a</sup> Naval Research Laboratory, 4555 Overlook Ave SW, Washington, DC 20375, USA

<sup>b</sup> National Research Council Postdoctoral Fellow at Naval Research Laboratory, 4555 Overlook Ave SW, Washington, DC 20375, USA

<sup>c</sup> Corning Incorporated, Lynn Morse Rd, Painted Post, NY 14870, USA

## ARTICLE INFO

### Article history:

Received 3 July 2017

Received in revised form 24 July 2017

Accepted 25 July 2017

### Keywords:

SIMS

AMS

SSAMS

Mass spectrometry

Trace elements

Isotopes

Spatial

Depth profile

## ABSTRACT

Secondary ion mass spectrometry (SIMS) provides spatially resolved trace analysis of solid materials, but can be complicated by unresolved abundant molecular isobars. By adding a 300-kV single-stage accelerator mass spectrometer (SSAMS) as a detector for a Cameca ims 4f SIMS, one can measure more abundant positive ions from the SIMS while removing molecular isobars, thus improving very low abundance trace element and isotope analysis. This paper describes important features and capabilities of such an integrated system at the Naval Research Laboratory using charge state +1 ions. Transmission loss is compared to molecule destruction as gas flow to the molecule-destruction cell increases. As most measurements tolerate more modest abundance sensitivities than for <sup>14</sup>C analysis, a lower gas flow is acceptable, so good transmission of 20–50% for ions of interest can be maintained for a broad range of ion masses. This new instrument has measured isotope ratios for uranium, lead, rare earths, and other elements from particulates and localized regions, with molecule destruction enabling the measurement at low SIMS mass resolving power and thus high transmission, as examples will show. This new and world-unique instrument provides improved capabilities for applications in nuclear and other forensics, geochemistry, cosmochemistry, and the development of optical, electronic, multifunctional, and structural materials.

Published by Elsevier B.V.

## 1. Introduction

While secondary ion mass spectrometry (SIMS) mass spectra are commonly complicated by contributions from molecular ions, techniques have been developed for trace element analysis by SIMS, for example as described for rare earth elements by Fahey [1]. These methods require known isotopic distributions, known effects of a sample energy offset on preferential molecular ion reduction, and a sufficient trace abundance. Such methods fail when the trace signal is much smaller than the uncertainty in that of deconvolved interfering molecular ions. This can occur if isotopic abundances or energy-offset effects are not well known, or if the molecular ion signals are comparatively too strong. Overcoming interferences by improving mass resolution with narrowed slits is inadequate for masses greater than  $\sim 90$  u, where an  $m/\Delta m > 10,000$  is usually required to resolve elemental and molecular ions, thereby reducing transmitted ion intensities too much. This is especially problematic for an intense molecular ion, where the tail in its distribution remains stronger than a nearby trace sig-

nal of interest. These problems are a major barrier to lower limits of detection by SIMS for trace impurities. The method is also rather complicated so not easy to perform.

Conversely, accelerator mass spectrometry (AMS) is a well-proven bulk analysis technique that eliminates interfering molecular ions, such as <sup>13</sup>CH from <sup>14</sup>C ion signals, for ultra trace measurements. Molecular ions are dissociated upon traversing a gas cell or thin foil without great loss in atomic ion transmission due to their high ion energy, typically in the MeV range. However, only a few AMS systems have been developed to measure trace elements in situ from solid materials, most with limited spatial resolution, as demonstrated by McDaniel, Anthony, Kirchhoff, Marble, Kim, Renfrow, Grannan, Reznik, Vizkelethy and Matteson [2]; Ender, Döbeli, Suter and Synal [3]; Wilson, Rucklidge, Kilius, Ding and Cresswell [4]. Only the Mega-SIMS at UCLA employs a commercial SIMS instrument to generate spatially correlated ions for analysis by AMS as described by Mao, Burnett, Coath, Jarzebinski, Kunihiro and McKeegan [5]; McKeegan, Kallio, Heber, Jarzebinski, Mao, Coath, Kunihiro, Wiens, Nordholt, Moses, Reisenfeld, Jurewicz and Burnett [6]. Furthermore, all these systems employ a tandem ion accelerator, which requires injection of negative ions not readily produced by most elements, and which produces multiple

\* Corresponding author.

E-mail address: [ken.grabowski@nrl.navy.mil](mailto:ken.grabowski@nrl.navy.mil) (K.S. Grabowski).

charge states of positive ions, thereby reducing detection efficiency.

To overcome the limitations described above, the Naval Research Laboratory (NRL) has combined a Cameca ims 4f SIMS with a  $\pm 300$ -kV single-stage AMS (SSAMS) from the National Electrostatics Corp. capable of measuring charge state +1 ions up to a mass of  $\sim 250$  u. By using a negative deck potential in the SSAMS, positive ions from the SIMS can be measured. Since the relative sensitivity factor (RSF) for most elements favors the use of positive ions (e.g., see Wilson, Stevie, Lux, Kirschbaum, Frank and Pallix [7]; Wilson, Stevie and Magee [8]; Wilson and Novak [9]), this mode improves the sensitivity for most trace impurities. By using a 300 kV accelerating potential, fewer charge states are produced following transit through Ar in the gas cell, with charge state +1 dominant. This also improves sensitivity. In addition, since “look alike” molecule fragments with the same magnetic rigidity as an element of interest must consist of lower mass, energy, and charge state ions, they cannot interfere because there is no charge state below +1. Further, higher charge state elemental ions from the SIMS are rare, and can only interfere with charge state +1 lighter elements with the same mass to charge ratio, in other words only for elements below  $\sim 120$  u. All these combined reasons provide an enhanced capability for trace element and isotope analysis of solid materials where spatial information is important. This paper demonstrates current capabilities with example measurements from the NRL SIMS-SSAMS facility.

## 2. Experimental procedure

A general description of the NRL facility and its mode of operation to measure U isotope ratios in oxide particulates is provided by Fahey, Groopman, Grabowski and Fazel [10]. In that work, a stationary defocused primary beam was directed at a particulate of interest, using optics similar to Köhler illumination of an optical microscope. Positive ions were extracted from the sample at 4.5 keV, mass analyzed by the SIMS, accelerated by 300 kV of the SSAMS, mass analyzed by the SSAMS using electrostatic peak switching (EPS) through the SSAMS magnet, and detected by the SSAMS electron multiplier (EM). A similar approach was used in the present work for bulk measurement of U ions from a piece of canary glass, so called due to its color caused by the presence of U, typically  $\sim 3\%$  by weight; of rare earth elements present in NIST SRM 610 multi-element reference glass with nominally 500 wppm of 61 elements; and of W isotopes from a W foil. For insulating samples, a thin high-purity (99.999%) gold coating was sputter deposited to minimize charging during analysis.

An alternative mode was used to obtain depth profiles in the present work. In this case, a focused primary  $^{16}\text{O}^-$  beam was deflected into a raster pattern to provide uniform erosion over a selected area. Secondary ions were selected from the center of the growing crater by a field aperture, positioned using the stigmatic imaging capability of the SIMS. Sputter times were converted to sample depth by measurement of the crater depth with a confocal microscope after completion of the measurement. Depth profiles were obtained from the outer surface of a glass tube that was extruded through a Nicrofer alloy die, to examine whether die components were incorporated into the glass surface. Quantitative analysis was performed using NIST SRM 610 and 612 glasses measured in a similar way to obtain suitable RSF values for Fe, Ni, and Cr, the expected contaminants. The stronger  $^{28}\text{Si}^+$  reference signal was measured in the SIMS Faraday cup, while weaker signals were measured by the electron multiplier at the end station of the SSAMS. The suitability of SIMS-SSAMS to examine trace contamination of Fe and Ni in silica glass, despite abundant  $\text{Si}_2^+$  ions of comparable masses, was demonstrated in Groopman, Fahey and

Grabowski [11], where  $\sim 30$  ppb Fe was measured in a Cameca Si-Ta grid standard sample, with the  $^{56}\text{Fe}^+$  signal only 10 ppm of the  $^{28}\text{Si}_2^+$  signal measured by the SIMS detector.

Since electrostatic peak switching through the SSAMS magnet can span  $\pm 6.5\%$  about a central mass, most measurements reported here were performed without changing the magnetic field of the SSAMS magnet. For the canary glass sample, two field settings were used; one to measure attenuation of  $^{238}\text{U}^+$ ,  $^{238}\text{U}^{16}\text{O}^+$ , and  $^{238}\text{U}^{16}\text{O}_2^+$  as a function of gas flow through the gas cell; another to measure  $^{238}\text{U}^+$  both as injected into the SSAMS, and as fragments from  $^{238}\text{U}^{16}\text{O}^+$  and  $^{238}\text{U}^{16}\text{O}_2^+$ , again as a function of gas flow through the gas cell.

Gas flow through the gas cell was converted into an effective gas thickness, using vacuum conductance calculations, dimensions of the gas cell structure, and pressure measured at the exit of the gas cell entering a turbomolecular pump. The gas thickness was used to evaluate a cross section for molecule destruction and scattering loss, based on the exponential decay constant of ion intensity with increasing gas thickness.

## 3. Results and discussion

### 3.1. Uranium ions from canary glass

As Fig. 1 shows for U-containing ions from canary glass, ion intensities diminish with increasing gas flow through the gas cell of the SSAMS, for both atomic and molecular ions injected into the SSAMS. Atomic ions are scattered by gas atoms, with some ions scattered outside the geometrical or energy acceptance of the spectrometer. Additionally, some may undergo a change of charge state (e.g., into a neutral), so are not transported through the SSAMS.

Besides the above effects, molecular ions can dissociate upon interaction with a gas atom. The kinetic energy of the molecule is then partitioned into its fragments, based upon their mass fraction of the molecule. Since the fragment has both lower mass and

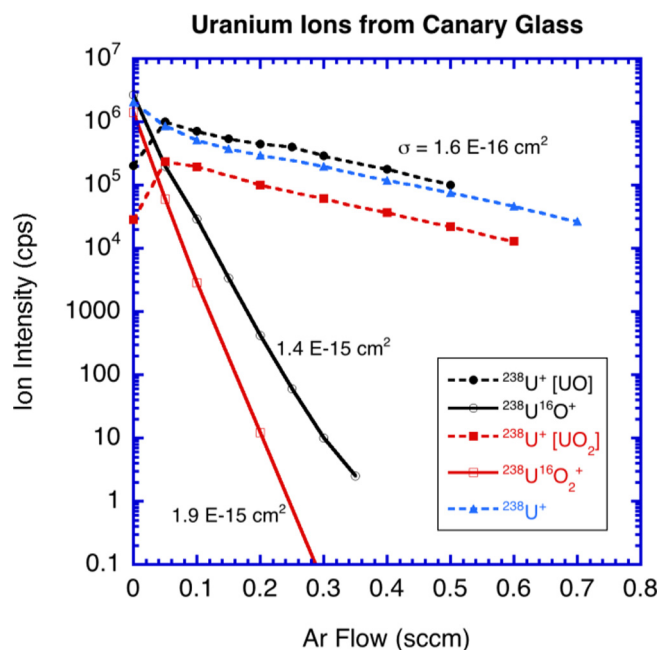


Fig. 1. Attenuation of U-containing ion intensities measured in SSAMS electron multiplier from canary glass as function of Ar gas flow through the SSAMS gas cell. Dashed lines depict atomic  $^{238}\text{U}^+$  ions as injected into SSAMS, from breakup of  $^{238}\text{U}^{16}\text{O}^+$ , or from breakup of  $^{238}\text{U}^{16}\text{O}_2^+$ . Solid lines depict molecular ions  $^{238}\text{U}^{16}\text{O}^+$  and  $^{238}\text{U}^{16}\text{O}_2^+$ . Cross section ( $\sigma$ ) for either scattering loss of atomic ions, or destruction of molecular ions is shown next to lines.

lower energy than the parent molecule, the SSAMS magnet and EPS settings must take both into account. The resulting molecule fragments then suffer the already mentioned attenuation effects.

The slope of a line in Fig. 1 represents an effective cross section for the observed attenuation. While the energy of  $^{238}\text{U}^+$  ions is somewhat different between the three sources of atomic ions, they all show nominally the same attenuation cross section ( $\sigma$ ) of  $1.6 \times 10^{-16} \text{ cm}^2$ . On the other hand, the cross section for destruction of molecular  $^{238}\text{U}^{16}\text{O}_2^+$  is a bit larger than that of  $^{238}\text{U}^{16}\text{O}^+$ , but both are about ten times greater than for atomic ions. This larger cross section for molecular ion attenuation allows their preferential reduction by  $\sim 10^4$ – $10^5$  compared to atomic ions, and enables trace level measurements of atomic ions. Because the molecule destruction cross section differed between the two molecules of Fig. 1, there are likely differences between other molecules as well. Thus, it is important to ascertain the gas flow required for a particular analysis effort.

### 3.2. Gadolinium isotopes in NIST SRM 610

Measurement of Gd isotopes (152, 154, 155, 156, 157, 158, 160) in rare-earth containing minerals, such as monazite ((La,Ce,Nd)PO<sub>4</sub>), is complicated by isobars of monoxides from lighter rare earth elements. But, because Gd has the largest neutron absorption cross section by an order of magnitude over all other elements ( $2.55 \times 10^5 \text{ b}$  for  $^{157}\text{Gd}$ ), this type of measurement may be useful to understand environmental exposure to neutrons and as a probe of s-process reaction rates in asymptotic giant branch (AGB) stars from measurements of extraterrestrial materials such as presolar grains, e.g., Zinner [12]. The monoxide isobars can be reduced using the SIMS-SSAMS approach, but some nuclear isobars remain. Prominent nuclear isobars of  $^{152}\text{Sm}$ ,  $^{154}\text{Sm}$ , and  $^{160}\text{Dy}$  obscure Gd at those masses, while less abundant nuclear isobars of  $^{156}\text{Dy}$  and  $^{158}\text{Dy}$  complicate measurement of Gd at those masses. Fortunately, there is no natural nuclear isobar at 155 or 157, and the longest-lived radioactive isobar  $^{157}\text{Tb}$  has a half-life of only 71 y.

Fig. 2 demonstrates monoxide interferences of concern from measurement of NIST SRM 610, and how increasing Ar flow in

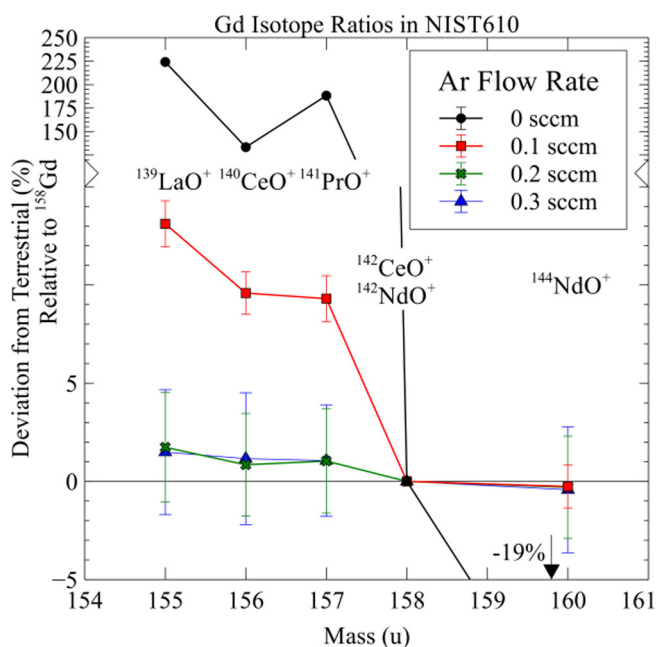


Fig. 2. Light rare-earth monoxide isobars can conflict with atomic Gd<sup>+</sup> ions measured from NIST SRM 610. But, these interferences are reduced as Ar gas flow increases from 0 to 0.3 sccm.

the gas cell reduces them significantly. This enables measurement of Gd isotope ratios normalized to  $^{158}\text{Gd}$  with only a few percent deviations from natural abundances. These deviations may reflect mass-dependent effects of the measurement technique. This measurement effort was much easier than the SIMS-only approach of Fahey (1998).

### 3.3. Iron, nickel, chromium contamination in extruded glass

Trace contamination of optical materials can alter their complex index of refraction and degrade desired properties, as described by Newns, Pantelis, Wilson, Uffen and Worthington [13]; Kitamura, Pilon and Jonasz [14]. Thus, there was concern that extrusion of glass through a die to make fibers may contaminate the surface with material from the die. Since the SIMS/SSAMS technique had demonstrated good sensitivity for Fe in silicon, as mentioned earlier, despite a potential interference from the  $^{28}\text{Si}_2^+$  ion, this approach seemed appropriate for glass that was extruded through a microfer die that contains Fe, Cr, and Ni. Fig. 3 shows the results obtained using 0.2 sccm of Ar flow through the gas cell. Although surface contamination is difficult to quantify due to transient effects during sputtering, it appears that concentrations near the percent level were present at the surface and extended near a micrometer deep. While the Ni level drops to a ppm, Cr penetrates a bit deeper and is about an order of magnitude higher. Iron drops at an intermediate rate, but persists at about the 20-ppm level, suggesting a residual contamination in the glass. Although atomic mixing during sputtering could have distorted the true depth profile of these impurities, contamination was clearly present near the surface. While high resolution SIMS ostensibly should be able to resolve interfering  $\text{Si}_2^+$  isobars from  $^{56}\text{Fe}^+$  and  $^{58}\text{Ni}^+$  (with  $m/\Delta m$  of 2950 and 3770, respectively), this is not easily the case when the molecular isobar is much more abundant than the impurities of interest, as in this example.

### 3.4. Peak shape symmetry problem

While evaluating early data collected at the SSAMS end station as shown in Fig. 4, we observed that measured peaks were rounded

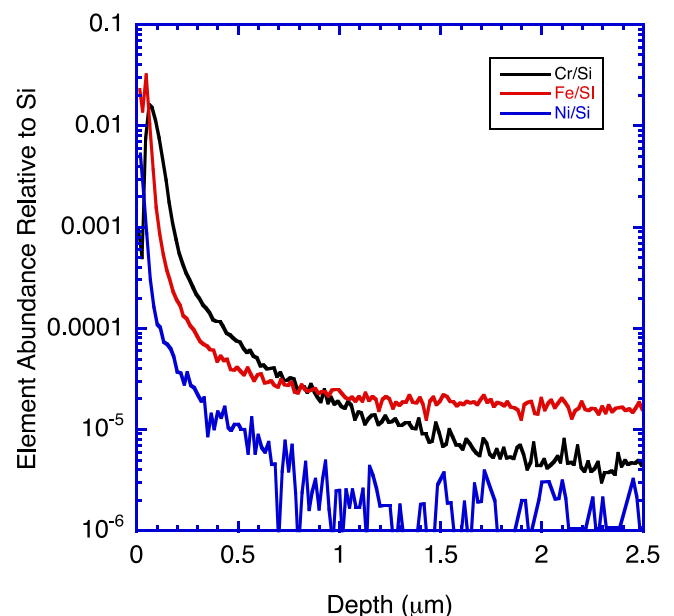
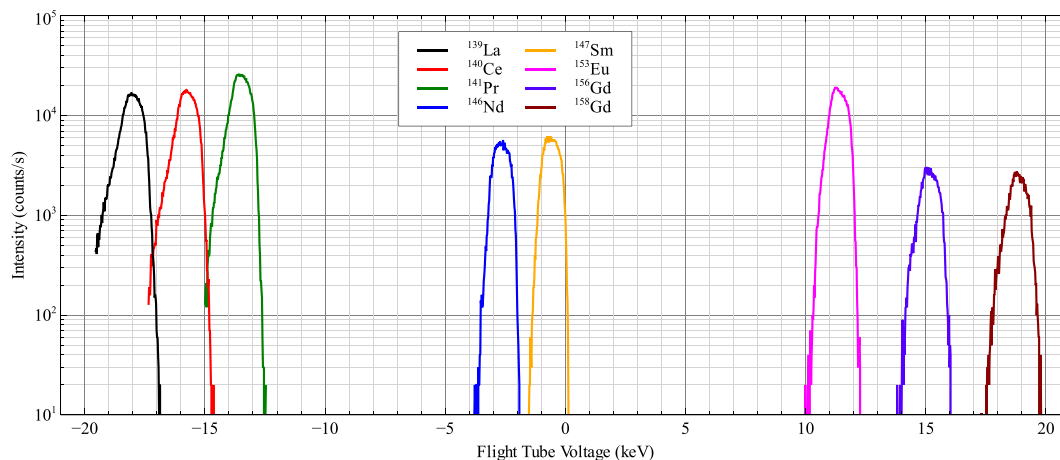


Fig. 3. Contamination of extruded glass surface by transfer of Fe, Ni and Cr from extrusion die.



**Fig. 4.** Electrostatic peak switching data measured for rare earth elements from  $^{139}\text{La}$  to  $^{158}\text{Gd}$  in NIST 610 SRM. Note the rounded tops for all peaks and asymmetrical and differing shapes at the extreme ends of the range.

at the top, and had a progressively asymmetric shape as the electrostatic potential on the SSAMS magnet flight tube increased. By using the beam imaging microchannel plate at the end station of the SSAMS, we observed that the beam shape did not expand symmetrically as the focusing Einzel lens of the injector was detuned, when the flight tube had a large potential. Instead a line beam was formed. In contrast, the expansion was symmetrical when the flight tube had no potential. This suggested an ion optics problem with the gap lenses at the entrance and exit of the SSAMS magnet, causing them to act somewhat like quadrupole lenses, focusing in one axis, defocusing in the other. Upon removing the coupling element between the magnet flight tube and the adjacent beam line that provides the gap lens, we discovered that the electrostatic gap was adjacent to the flight tube flange. As Fig. 5 shows, the rectangular opening was quite close to the face of that flange. Simion modeling for this geometry confirmed that asymmetric focusing would result.

After inverting the orientation of the gap to face the upstream beamline with a circular opening, beam optics were greatly improved. As Fig. 6 shows for W isotope peaks collected from a W foil, the peaks have very flat tops and a uniform shape over a broad range of electrostatic potentials on the flight tube. We expect this improved performance will enhance our measurement precision.

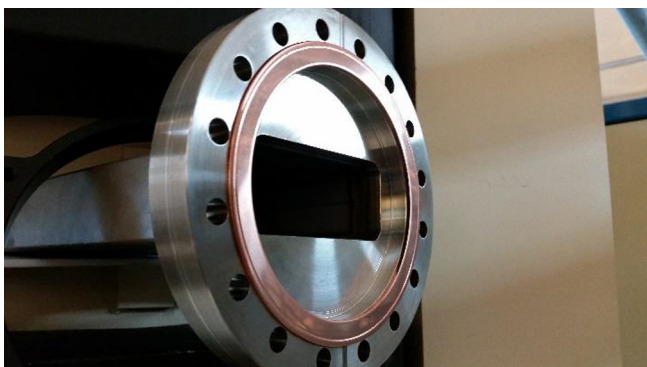


**Fig. 5.** Image of entrance into flight tube of SSAMS magnet. Note the proximity of the rectangular opening to the flange face.

### 3.5. Modeling effects of different stripper gases

Thus far our measurements have used Ar in our gas cell to dissociate molecules. However, previous work with light ions by Hvelplund, Lægsgaard and Horsdal Pedersen [15], Schulze-König, Seiler, Suter, Wacker and Synal [16] and Maxeiner, Seiler, Suter and Synal [17] suggests He may be a preferable gas since it should scatter ions less, thus reducing transmission loss, while still dissociating molecules and producing predominantly charge state +1 ions. Recent work using He gas for heavy ions Vockenhuber, Alfimov, Christi, Lachner, Schulze-König, Suter and Synal [18] also shows promise for similar reasons.

To better understand the implications of using different gases, simple modeling of ion scattering was performed, following modeling ideas of Maxeiner, Suter, Christl and Synal [19] for C ions incident on He. The cross section was computed for scattering of 300 keV ions using the Lenz-Jensen potential, and the probability calculated for ions to scatter less than 14.1 mrad in a single scatter event, i.e., within the acceptance of the SSAMS magnet, given a gas thickness of  $1 \times 10^{16}$  at/cm<sup>2</sup> as is typically used. Fig. 7a shows the results of this calculation. For the heavier ions incident on Ar, a transmission of about 50% would be expected from a single scatter event. By comparison, the measured transmission was about 20–30% for heavy ions incident on Ar. This reflects the importance of multiple scattering events and the possibility of a charge state change of the injected ion. In contrast, the calculated transmission would be about 90% if He were the scattering atom. The importance of multiple scattering events and charge state change from He interactions remains to be determined for our system.

Another aspect of a scattering event is the energy loss of the incident ion. This is important to know as it impacts transmission through the spectrometer and influences mass resolution. Therefore, the maximum energy loss experienced in a single scattering event was calculated using a maximum acceptance angle of the spectrometer of 14.1 mrad. Only forward scattering in the center of mass system was considered, since the energy loss for backward scattering is so large and the interaction so unlikely it was considered unimportant in this analysis. The results of the computation for a range of ion masses and target atoms from H to Ar are shown in Fig. 7b. Contrary to intuition, the maximum energy loss increases with decreasing mass of the target atom. While the maximum energy loss is only  $\sim 300$  eV for the heaviest ions on Ar, it is  $\sim 4$  keV for those ions on He. This is because it requires a closer and more energy draining interaction for a light atom to scatter a heavier ion to such a large angle. While this behavior is somewhat

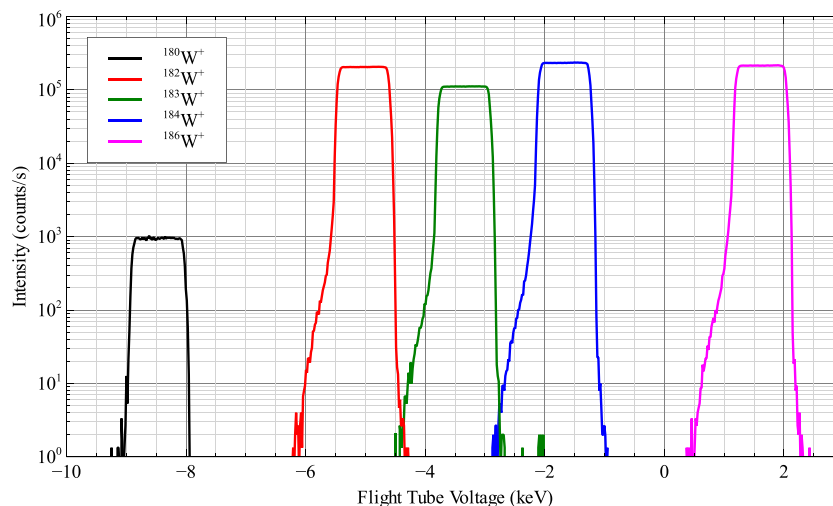


**Fig. 6.** Electrostatic peak switching data measured for W isotopes from a W foil, after inversion of gap lens. Note broad flat-topped peaks and consistent peak shape across range of flight tube voltages.

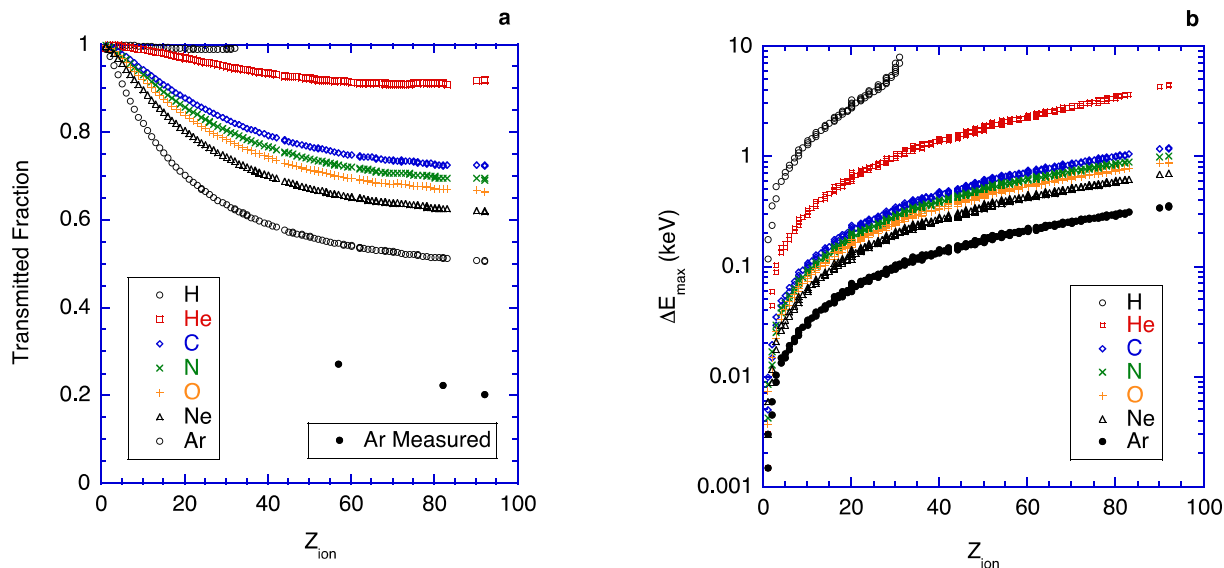


**Fig. 7.** Modeling effects of single scatter of 300 keV atomic ions of different  $Z$  on a range of atoms from H to Ar. (a) Shows the transmission expected from the model, as well as data measured for  $^{139}\text{La}^+$ ,  $^{208}\text{Pb}^+$  and  $^{238}\text{U}^+$  ions interacting with Ar gas. (b) Shows the maximum energy loss for ions transmitted, consistent with the largest scattering angle possible for measurement. Contrary to intuition, the largest energy loss increases with decreasing target atom mass.

counter intuitive and potentially of concern, its impact is diminished by the much lower cross section for such close interactions. Nevertheless, one needs to be aware of this behavior when selecting the gas to use in the gas cell.

#### 4. Conclusions

The examples provided demonstrate that ppm level impurities can be measured by selective elimination of molecular isobar interferences using the combined SIMS–SSAMS system at NRL and sufficient gas flow through the molecule destroying gas cell. Further, the technique is simple, without need of high resolution by SIMS, sample energy offset, or deconvolution of molecular-isobar interferences. Essentially, the SSAMS is a molecule-insensitive SIMS detector. As such, the combined instrument provides the mass-resolved imaging and depth-profiling capabilities of conventional SIMS, but without the clutter of interfering molecular ions. With discovery of the ion optical defect described in section 3.4, we have

improved precision from our initial data, and hope to improve it further by optimizing our choice of gas and its flow for the molecule destroying gas cell.

#### Acknowledgements

The authors acknowledge the Office of Naval Research and the Naval Research Laboratory for their support to develop this facility, and the significant contributions from Mr. Victor Cestone to set up and maintain the laboratory and instrument. They also thank Dr. Shyam Bayya for providing extruded glass samples for analysis.

#### References

- [1] A.J. Fahey, Details of the measurement of rare earth and other trace element abundances by secondary ion mass spectrometry, *Int. J. Mass Spectrom.* 176 (1998) 63–76.
- [2] F.D. McDaniel, J.M. Anthony, J.F. Kirchoff, D.K. Marble, Y.D. Kim, S.N. Renfrow, B.C. Grannan, E.R. Reznik, G. Vizkelethy, S. Matteson, Impurity determination

- in electronic materials by accelerator mass spectrometry, *Nucl. Instr. Methods Phys. Res. B*, 1994; 89, 242–249.
- [3] R.M. Ender, M. Döbeli, M. Suter, H.-A. Synal, Accelerator SIMS at PSI/ETH Zurich, *Nucl. Instrum. Methods Phys. Res. B* 123 (1997) 575–578.
- [4] G.C. Wilson, J.C. Rucklidge, L.R. Kilius, G.-J. Ding, R.G. Cresswell, Precious metal abundances in selected iron meteorites: in-situ AMS measurements of the six platinum-group elements plus gold, *Nucl. Instrum. Methods Phys. Res. B* 123 (1997) 583–588.
- [5] P.H. Mao, D.S. Burnett, C.D. Coath, G. Jarzebinski, T. Kunihiro, K.D. McKeegan, MegaSIMS: a SIMS/AMS hybrid for measurement of the Sun's oxygen isotopic composition, *Appl. Surf. Sci.* 255 (2008) 1461–1464.
- [6] K.D. McKeegan, A.P. Kallio, V.S. Heber, G. Jarzebinski, P.H. Mao, C.D. Coath, T. Kunihiro, R.C. Wiens, J.E. Nordholt, R.W. Moses Jr., D.B. Reisenfeld, A.J. Jurewicz, D.S. Burnett, The oxygen isotopic composition of the Sun inferred from captured solar wind, *Science* 332 (2011) 1528–1532.
- [7] R.G. Wilson, F.A. Stevie, G.E. Lux, C.L. Kirschbaum, S. Frank, J. Pallix, Depth profiles, projected ranges, and secondary ion mass spectrometry relative sensitivity factors for more than 50 elements from hydrogen to uranium implanted into metals, *Surf. Coat Technol.* 51 (1992) 358–363.
- [8] R.G. Wilson, F.A. Stevie, C.W. Magee, *Secondary Ion Mass Spectrometry: A Practical Handbook for Depth Profiling and Bulk Impurity Analysis*, John Wiley & Sons, New York, 1989.
- [9] R.G. Wilson, S.W. Novak, Systematics of secondary-ion-mass spectrometry relative sensitivity factors versus electron affinity and ionization potential for a variety of matrices determined from implanted standards of more than 70 elements, *J. Appl. Phys.* 69 (1991) 466–474.
- [10] A.J. Fahey, E.E. Groopman, K.S. Grabowski, K.C. Fazel, Measurement of uranium isotopes in particles of U3O8 by secondary ion mass spectrometry-single-stage accelerator mass spectrometry (SIMS-SSAMS), *Anal. Chem.* 88 (2016) 7145–7153.
- [11] E.E. Groopman, A.J. Fahey, K.S. Grabowski, Trace element determination in presolar grains with the NRL SIMS-SSAMS, *Meteorit Planet Sci* 51 (2016) A298.
- [12] E. Zinner, 1.4 – Presolar Grains A2 – Holland, Heinrich D, in: K.K. Turekian (Ed.) *Treatise on Geochemistry* (second ed.), Elsevier, Oxford, 2014, pp. 181–213.
- [13] G.R. Newns, P. Pantelis, J.L. Wilson, R.W.J. Uffen, R. Worthington, Absorption losses in glasses and glass fibre waveguides, *Opto-electronics* 5 (1973) 289–296.
- [14] R. Kitamura, L. Pilon, M. Jonasz, Optical constants of silica glass from extreme ultraviolet to far infrared at near room temperature, *Appl. Opt.* 46 (2007) 8118–8133.
- [15] P. Hvelplund, E. Lægsgaard, E. Horsdal, Pedersen Equilibrium charge distributions of light ions in helium, measured with a position-sensitive open electron multiplier, *Nucl. Instrum. Methods* 101 (1972) 497–502.
- [16] T. Schulze-König, M. Seiler, M. Suter, L. Wacker, H.A. Synal, The dissociation of 13CH and 12CH2 molecules in He and N2 at beam energies of 80–250 keV and possible implications for radiocarbon mass spectrometry, *Nucl. Instrum. Methods Phys. Res. Sect. B* 269 (2011) 34–39.
- [17] S. Maxeiner, M. Seiler, M. Suter, H.-A. Synal, Charge state distributions and charge exchange cross sections of carbon in helium at 30–258 keV, *Nucl. Instrum. Methods Phys. Res. Sect. B* 361 (2015) 541–547.
- [18] C. Vockenhuber, V. Alfimov, M. Christl, J. Lachner, T. Schulze-König, M. Suter, H. A. Synal, The potential of He stripping in heavy ion AMS, *Nucl. Instrum. Methods B* 294 (2013) 382–386.
- [19] S. Maxeiner, M. Suter, M. Christl, H.A. Synal, Simulation of ion beam scattering in a gas stripper, *Nucl. Instrum. Methods B* 361 (2015) 237–244.